44th AIAA Aerospace Sciences Meeting and Exhibit
9 - 12 January 2006, Reno, Nevada

AIAA 2006-115

An Evaluation of the Partially-Resolved Numerical Simulation Procedure For Near-Wall Turbulence Prediction

Xiaodan Cai*, Foluso Ladeinde†

Thaerocomp Technical Corporation, P.O. Box 1527, Stony Brook, NY 11790

In this paper, we attempt to evaluate the newly-proposed PRNS procedures for near-wall turbulence prediction. The PRNS procedure is combined with the low-Reynolds number turbulent model (Abid's version) to calculate the near-wall turbulent structures in two-dimensional flat-plate boundary flows, two-dimensional and three-dimensional backard-facing step flows. We have found that the PRNS procedure with the fixed model constant ($R_{cp} = 0.38$) generally predicts weaker turbulent structures as compared to its corresponding RANS model. It is suspected that the near-wall grid size may not be suitable for the PRNS calculations with $R_{cp} = 0.38$. More studies are surely needed on this subject. Furthermore, the capability and usefulness of the PRNS procedures on resolving large-scale energetic turbulent structures require further evaluations.

I. Introduction

High-Reynolds number turbulent flows pose significant computational challenges for CFD-aided design calculations of realistic aerospace system components. The Reynolds-Averaged Navier-Stokes (RANS) modeling, commonly used today for practical applications, has frequently proved to be poorly adapted to handle complex turbulent flows with massive separation. While the Large-Eddy Simulation (LES) procedure has shown the ability to resolve flow structures and achieve more accurate predictions, it is too costly for realistic engineering applications. As a comprise between RANS and LES, a class of hybrid RANS-LES methods has been proposed, among which detached eddy simulation **(**DES) has shown some impressive results for complex aerodynamic applications.[1-3]

Unfortunately, the standard DES procedure introduces significant grid dependency into the RANS portion of the simulations, which requires the grid-spacing of wall grids in the tangential directions larger than the boundary layer thickness at that location. This is usually the lower limit for the DES grid resolution, which may easily be violated in industrial simulations. Further grid refinement below this limit can result in a grid induced-separation (GIS), as pointed out by Menter et al.[4] In order to resolve this issue, a modified DES and other RANS-LES approaches might be necessary. One of the principal aims in the present paper is to evaluate the recently-proposed partially-resolved numerical simulation (PRNS)[5-9] as a candidate that does not have the setbacks of the DES approach.

PRNS is intended to provide a unified simulation strategy (from RANS to LES) for high Reynolds number complex turbulent flows.[5, 6] The governing equations for the PRNS method are the temporally-filtered Navier-Stokes equations, in which the dependent variables can be construed as the statistical mean (as in RANS), or the partially resolved large-scale (as in LES), or the instaneous (as in DNS) values of turbulence, while the effects of unresolved scales are modeled based on the size of the temporal filtering. As pointed out by Shih and Liu[5], various types of models (zero-, one- and two-equation models, etc.) such as those used in traditional RANS can be used for the unresolved stresses and fluxes. In their original papers,[5, 6] Shih and Liu tested a high-Reynolds number k-ε model to model these terms, in which k, the kinetic energy of the unresolved scales, and ε, its dissipation rate are governed by the traditional RANS equations. However, a "resolution control parameter", R_{cp} has been introduced to regulate the

*Senior Research Engineer, AIAA Member.
† Director of Research, AIAA Life Member and Associate Fellow.

relative content of the resolved and unresolved scales. By fixing R_{cp} during a PRNS calculation, Shih and Liu found that the grid dependency issues caused by spatial filtering could be avoided.

The preliminary results presented by Shih and Liu[5, 6] for pipe flow and LM6000 combustor are very encouraging, in the sense that the model fairly resolves the large-scale turbulence structures away from the wall region. However, their calculations did not captured the near-wall features because they used wall functions. Also, it was not discussed whether or not the "resolution control parameter" R_{cp} should be regulated or kept fixed if the meshes were varied for a given physical problem. Shih and Liu used a value of 0.38 for R_{cp} for a wide range of Reynolds number and reported a good agreement between PRNS results and results from experiments/DNS. It is the intention in the present work to evaluate the procedure for near-wall features using low-Reynolds number k-ε models for the unresolved stress calculations. The low-Reynolds number k-ε model by Abid[10] is used in our work for this purpose, and we investigate the performance of PRNS for near-wall flows. We are not aware of previous work on PRNS that has addressed the near-wall problem. We are also investigating the value of 0.38 used for R_{cp} on its generality, with the hope of coming up with a fairly, globally optimum, value.

II. PRNS Modeling

The governing equations for the PRNS modeling are the temporally-filtering Navier-Stokes equations:

$$\frac{\partial}{\partial t}\overline{\rho} + \frac{\partial}{\partial x_i}\left(\overline{\rho}\cdot\widetilde{u}_i\right) = 0, \tag{1}$$

$$\frac{\partial}{\partial t}\left(\overline{\rho}\widetilde{u}_i\right) + \frac{\partial}{\partial x_j}\left(\overline{\rho}\widetilde{u}_i\cdot\widetilde{u}_j\right) = -\frac{\partial}{\partial x_i}\overline{p} - \frac{\partial}{\partial x_j}\tau_{ij} + \frac{\partial}{\partial x_j}\left(2\overline{\mu}\widetilde{S}_{ij} - \frac{2}{3}\delta_{ij}\overline{\mu}\widetilde{S}_{kk}\right), \tag{2}$$

$$\frac{\partial}{\partial t}\left(\overline{\rho}\widetilde{e}\right) + \frac{\partial}{\partial x_i}\left(\overline{\rho}\widetilde{u}_i\cdot\widetilde{e}\right) = \overline{pS_{kk}} - \frac{\partial}{\partial x_j}q_j + \frac{\partial}{\partial x_j}\left(\overline{\kappa}\frac{\partial}{\partial x_j}\widetilde{T}\right) + \left(2\overline{\mu}\overline{S_{ij}S_{ij}} - \frac{2}{3}\overline{\mu}\overline{S_{kk}S_{kk}}\right), \tag{3}$$

where $S_{ij} = \left(\frac{\partial u_i}{\partial x_j} + \frac{\partial u_j}{\partial x_i}\right)/2$, and ρ, u_i, T, p and e are the density, velocity, temperature, pressure and internal energy, respectively. In the terminology of PRNS averaging, the filtered quantities, $\overline{\phi}$ are defined in time domain as

$$\overline{\phi}(t, x_i) = \int_T \phi(t', x_i)G(t - t')dt'. \tag{4}$$

and $\widetilde{\phi}$ is its density-weighted counterpart.

With a top-hat filtering function used for G, Equation (4) becomes

$$\overline{\phi}(t, x_i) = \frac{1}{\Delta T}\int_{t-\Delta T/2}^{t+\Delta T/2}\phi(t', x_i)dt'. \tag{5}$$

As $\Delta T \to \infty$, Equation (5) becomes the traditional Reynolds-averaging. For a finite ΔT, Equation (5) represents mainly the large scales of turbulence. The PRNS averaging thus regulates the contents of resolved and unresolved turbulent scales by the size of the time intervals instead of the size of grids, which is different from the other hybrid RANS/LES models and provides the opportunity for grid-independent calculations.

It is noted that in Equations (1) through (3), there are several unclosed terms, including the turbulent stress (τ_{ij}), the turbulent heat fluxes (q_i), the pressure-dilation correlation terms ($\overline{pS_{kk}}$), and the compressible turbulence kinetic energy dissipation rates ($2\overline{\mu}\overline{S_{ij}S_{ij}} - \frac{2}{3}\overline{\mu}\overline{S_{ii}S_{kk}}$). The pressure-dilation correlation terms and compressible dissipation rates, which represent the effects of flow compressibility, are negligible for the current low Mach number flows[11, 12]. For the turbulent stress (τ_{ij}) and the turbulent fluxes (q_i), Shih and Liu used a high-Reynolds number *k-ε* model with the parameter R_{cp} to regulate the contents of the resolved and unresolved turbulent scales as

$$\tau_{ij} = -2\mu_T\left(\widetilde{S}_{ij} - \frac{1}{3}\delta_{ij}\widetilde{S}_{kk}\right) + \frac{1}{3}\delta_{ij}\tau_{kk}, \tag{6}$$

$$q_i = -\kappa_T \frac{\partial \widetilde{T}}{\partial x_i}, \tag{7}$$

where the model coefficients are

$$\mu_T = R_{cp}(\Delta T)\cdot C_\mu \overline{\rho}\frac{k^2}{\varepsilon}, \kappa_T = \mu_T / \mathrm{Pr}_t, \tag{8}$$

μ_T is the turbulence viscosity, ΔT is the temporal filter width, κ_T is the turbulent diffusivity, Pr_t is the turbulent Prandtl number, and C_μ is the standard model constant in the *k-ε* model. To account for the near-wall features, we use Abid's low-Reynolds number *k-ε* model to model the turbulent kinetic energy, *k* and its dissipation rate, *ε*, which are obtained from

$$\frac{\partial k}{\partial t} + \widetilde{u}_j\frac{\partial k}{\partial x_j} = \frac{1}{\rho}\tau_{ij}\widetilde{S}_{ij} - \varepsilon + \frac{1}{\rho}\frac{\partial}{\partial x_j}\left(\left(\widetilde{\mu} + \frac{\widetilde{\mu}_t}{\sigma_k}\right)\frac{\partial k}{\partial x_j}\right), \tag{9}$$

$$\frac{\partial \varepsilon}{\partial t} + \widetilde{u}_j\frac{\partial \varepsilon}{\partial x_j} = \frac{1}{\rho}C_{\varepsilon 1}\frac{\varepsilon}{k}\tau_{ij}\widetilde{S}_{ij} - C_{\varepsilon 2}f_2\frac{\varepsilon}{k}\varepsilon + \frac{1}{\rho}\frac{\partial}{\partial x_j}\left(\left(\widetilde{\mu} + \frac{\widetilde{\mu}_t}{\sigma_\varepsilon}\right)\frac{\partial \varepsilon}{\partial x_j}\right). \tag{10}$$

The model constants for Abid's model are:

$$C_\mu = 0.09,$$
$$C_{\varepsilon 1} = 1.45, \quad \sigma_k = 1.0,$$
$$C_{\varepsilon 2} = 1.83, \quad \sigma_k = 1.4.$$

Also, we have

$$f_\mu = \left[1 + \frac{4}{R_t^{0.75}}\right]\tanh\left(0.008\cdot \mathrm{Re}_k\right),$$

$$f_2 = \left(1 - \frac{2}{9}\exp\left(-\frac{R_t^2}{36}\right)\right)\cdot\left(1 - \exp\left(-\frac{\mathrm{Re}_k}{12}\right)\right),$$

where $\mathrm{Re}_k = \frac{\rho\sqrt{k}d}{\mu}\cdot\mathrm{Re}$ and *d* is the distance to the nearest wall.

It should be noted that the Reynolds-averaged stress, R_{ij}, has contributions from both the resolved and unresolved scales. Since the PRNS variables are time-filtered, quasi-stationary flow states are needed for calculating the Leonard stress for the resolved scales.[6]

III. Numerical Method

We use a high-order finite-difference scheme in a curvilinear coordinate system. In standard notations, the filtered equations can be written as

$$\frac{\partial \hat{U}}{\partial t}+\frac{\partial}{\partial \xi}\left(\hat{F}-\frac{1}{\mathrm{Re}}\hat{F}_v\right)+\frac{\partial}{\partial \eta}\left(\hat{G}-\frac{1}{\mathrm{Re}}\hat{G}_v\right)+\frac{\partial}{\partial \xi}\left(\hat{H}-\frac{1}{\mathrm{Re}}\hat{H}_v\right)=0, \tag{11}$$

By using the implicit, approximately-factored finite-difference algorithm of Beam-Warming and employing Newton-like sub-iterations, we have the following numerical algorithms:

$$\begin{aligned}
&\left[J^{-1^{p+1}}+\phi^i\Delta t_s\delta_\xi\left(\frac{\partial \hat{F}^p}{\partial U}-\frac{1}{\mathrm{Re}}\frac{\partial \hat{F}_v^p}{\partial U}\right)\right]J^{p+1}\times\left[J^{-1^{p+1}}+\phi^i\Delta t_s\delta_\eta\left(\frac{\partial \hat{G}^p}{\partial U}-\frac{1}{\mathrm{Re}}\frac{\partial \hat{G}_v^p}{\partial U}\right)\right]J^{p+1}\times\\
&\qquad\left[J^{-1^{p+1}}+\phi^i\Delta t_s\delta_\zeta\left(\frac{\partial \hat{H}^p}{\partial U}-\frac{1}{\mathrm{Re}}\frac{\partial \hat{H}_v^p}{\partial U}\right)\right]\Delta U\\
&=-\phi^i\Delta t_s\left[J^{-1^{p+1}}\frac{(1+\phi)U^p-(1+2\phi)U^n+\phi U^{n-1}}{\Delta t}-U^p\left(\left(\frac{\xi_t}{J}\right)_\xi+\left(\frac{\eta_t}{J}\right)_\eta+\left(\frac{\zeta_t}{J}\right)_\zeta\right)\right]\\
&\qquad-\phi^i\Delta t_s\left[\delta_\xi\left(\hat{F}^p-\frac{1}{\mathrm{Re}}\hat{F}_v^p\right)+\delta_\eta\left(\hat{G}^p-\frac{1}{\mathrm{Re}}\hat{G}_v^p\right)+\delta_\zeta\left(\hat{H}^p-\frac{1}{\mathrm{Re}}\hat{H}_v^p\right)\right],
\end{aligned} \tag{12}$$

where

$$\phi^i=\frac{1}{1+\phi},\ \Delta U=U^{p+1}-U^p,$$

and superscripts "*p*" and "*n*" denote the sub-iteration steps and the time steps, respectively. In the above equations, (ξ, η, ς) are the curvilinear coordinates and Δt_s is the time step for the sub-iterations. Either a first or second-order temporal accuracy can be specified in the above iterative procedure by selecting $\phi=0$ or $\phi=1/2$, and p is the sub-iteration index. For $p=1$, $U^p=U^n$ and as $p\to\infty$, $U^p\to U^{n+1}$. This dual time-step procedure is not only good for time-accurate simulations, but it also is good to speed-up the convergence rate for a steady-state solution. The above flow solver is then coupled with the first-order, upwinding scheme to solve the transport equations for *k* and *ε*.

IV. The Test Cases

The first case uses a spatially-developing flat-plate boundary layer flow to evaluate the near wall performance of PRNS using a low-Reynolds number *k-ε* model. A flat-plate with leading-edge was initially immersed in a uniform flow with zero pressure gradient at $Ma_\infty=0.3$ and $\mathrm{Re}_\infty=6\times10^6$ per unit length. The mean flow is two-dimensional and there are no fluctuations imposed on the mean flows. The mesh size is 65 x 97. The flat plate is unity in length. Symmetry boundary conditions are imposed on a region of length *x*=0.333 in front of the plate. Computational domain height is approximately 1.0, minimum normal grid spacing at the wall is 1×10^{-6}, and the grid is stretched at a rate of 1.18 until the vertical spacing just exceeds the horizontal spacing. The horizontal spacing is constant at $\Delta x=0.0208333$. In this paper, no grid sensitivity studies have been performed and the first grid size used is assumed fine enough for typical RANS calculations ($y^+\equiv\frac{\rho y\cdot u^*}{\mu}\approx0.2$, where u* is the friction velocity). Figure 1 shows the effects of R_{cp} on the mean profile at three spatial locations. The PRNS calculations shown here use $R_{cp}=0.38$. For comparison, Figure 1 also shows the results obtained from the Spalart-Allmaras (S-A) model and the DES model. It can be seen that the PRNS velocity profiles are slightly higher than the theoretical profile (White[14]), while the original Abid model (R_{cp}=1.0) compares better with the theory. The DES model almost reproduces the results obtained from the original Spalart-Allmaras model. This is not surprising considering the fact that the transition grid size for the DES model is very big ($d_t^+\approx2700$) and most part of the boundary flows are

simply calculated by the near-wall RANS model. Figure 2 compares the surface skin friction for various turbulent models with the theoretical curves (solid lines). It can be seen that the effect of R_{cp} is to reduce the values of the skin friction. The difference between the PRNS's predictions and the original Abid model's is approximately 17%, but the difference is only 6% compared to the theoretical results (lower curve). Therefore, it seems that the values of R_{cp} used in PRNS method do affect the near-wall predictions but in a mild way.

The second test case is based on the backward-facing step flow from Driver and Seegmiller's experiment.[15] This flow has been used as an important test case in many RANS calculations for examining the effects of near-wall treatment on separated flows.[16] In the experiment, several different upper wall inclinations were tested, but in the current simulation, the upper wall was kept horizontal (zero degree). The test conditions are $Ma = 0.128$, and $\mathrm{Re}_h = 37573$ per unit step height, *H*. A one-zone mesh (165×185) is used for both Abid's model and the PRNS calculations, and the computational domain extents from *x/H*=-4.0 upstream to *x/H*=35 (see Figure 3). Clustered grids are used near the solid walls with $y^+ \equiv \frac{\rho y \cdot u^*}{\mu} \approx 1.2$. Since this flow is modeled using a single zone, the step itself is modeled using a viscous wall boundary around a hole. The same inlet density, velocity, and turbulent kinetic energy are used for both PRNS and Abid's model calculations, which are interpolated from the flat-plate results calculated (above) using Abid's model at the streamwise location with $\mathrm{Re}_x = 4.5 \times 10^6$, and rescaled to match the experimental data. Figure 4 presents the prescribed inlet U-velocity and the turbulent kinetic energy compared to experimental data. The definition, $k = 0.75(\overline{uu} + \overline{vv})$ is used to calculate the turbulent kinetic energy of the experimental data. The inlet pressure was extrapolated from the interior of the domain. To specify the inlet turbulent dissipation rate for PRNS calculations, two approaches were tested: $\varepsilon_0^{(PRNS)} = \varepsilon_0^{(Abid)}$, and $\varepsilon_0^{(PRNS)} = R_{cp} \cdot \varepsilon_0^{(Abid)}$ which is equivalent to using $\mu_{T0}^{(PRNS)} = \mu_{T0}^{(Abid)}$. We found that the second approach works better for PRNS calculations, and are presented in the following. The primary re-attachment lengths from both the PRNS and Abid's model are listed in Table 1, where the numerical results from Menter's SST model [17], Spalart-Allmaras's (S-A) model[18] and DES models are also included here for comparison. The weaker turbulent viscosity (implied in the PRNS method based on Abid model and in the DES model with small transition grid-size, $d_t^+ \approx 100$) seems to over-predict the re-attachment length. Similarly, the PRNS model based on the standard high-Reynolds-number k-ε model (noted as HR model in the table) also over-predicts the re-attachment length. It is noted that for both the standard high-Reynolds-number k-ε model and its PRNS derivative, coarse grids (116×102) have been used and the near-wall grid-size is $y^+ \equiv \rho y \cdot u^* / \mu \approx 25$. Figure 5 below compares the velocity vector plots from PRNS with RANS and DES results. It clearly demonstrates that the PRNS models and the DES model with $d_t^+ \approx 100$ generate larger recirculation zones and that the streamlines around the recirculation zones are oscillatory.

Table 1: Re-attachment lengths of the backward-facing step flows

Model	Abid	PRNS (Abid)	HR	PRNS (HR)	DES ($d_t^+ \approx 100$)	DES ($d_t^+ \approx 2200$)	S-A	SST	Exp
Xr/H	6.00	8.25	6.00	8.50	10.20	6.25	5.75	5.25	6.25

The prediction of the skin friction coefficient along the step wall by PRNS and various RANS and DES models are given in Figure 6. It can be seen that the PRNS models (based on low-Re k-ε model or high-Re k- ε model) can not accurately predict the location of re-attachment length, while their corresponding RANS models show a better prediction both near and away from the re-attachment points. It is observed that the DES model with $d_t^+ \approx 100$ also shows an oscillatory skin friction coefficient as the PRNS models. Figure 7 present the mean velocity profiles at two downstream locations (*x/H*=1.0 and *x/H*=2.5). It again shows that the PRNS treatment based on the low-Re k-ε model gives a behaviour that is similar to the one based on the high-Re k-ε model. Figure 8 presents the turbulent-stress ($-\overline{uv}$) profiles at two typical downstream locations, of which one is located inside the recirculation zone

(X/H=2.5) and one is outside the recirculation zone (*x/H*=10). It is observed that Abid's model performs a little better than the other models, which is the reason that drives us to use Abid's model as the base model for PRNS. Figure 8 also shows that the PRNS model predicts a much weaker turbulent stress than the RANS models. Considering that PRNS is a procedure intended for large-eddy simulations of very complex turbulent flows, the total turbulent stresses should consist of two contributions, one is from the resolved scales (Leonard stress, L_{ij}) and the other from the modeled unresolved scales (τ_{ij}), i.e., $T_{RANS} = L_{ij} + \tau_{ij}$. Since we haven't imposed any turbulent fluctuations in our 2D simulations, it is not very surprising that no large-scale turbulent structures occur in the simulated backward-facing step flows. In other words, this means that Leonard stresses are non-existent in our PRNS calculations, which explains why the turbulent stresses predicted by the PRNS calculations are much weaker.

It is our choice to simulate 3D backward-facing step flows with the hope that significant large-scale turbulent structures will occur and be captured by the PRNS procedures. The computational domain in our 3D calculations is a simple extension of the 2D geometry in the spanwise direction. The grid size is 165×185×22 with $\delta z = 0.1$. It is noted that from Figures 9 and 10, both the 3D RANS and PRNS calculations produce only steady-state two-dimensional flow structures, and the PRNS model predicts a weaker turbulent stress than the RANS model. Figure 11 compares the friction coefficient obtained from 2D and 3D RANS and PRNS calculations. It is interesting to note that the PRNS calculations predict better results up to *X/H*=5, and then show a lag in the development of the friction coefficient. The lack of 3D large-scale energetic turbulent structures, somewhat surprising, is believed be the reason for the weaker turbulent stress and large recirculation zones for the PRNS calculations. It is worthy to point out that in our 3D simulations, we didn't impose any turbulent fluctuations. Due to the computer costs, we haven't investigated the situations with turbulent fluctuations imposed initially. It is also noted that, in the current calculations, we use the same grid sizes for both the RANS and the PRNS calculations. We thus suspect that the grid sizes are unsuitable for the PRNS calculations to develop the unsteady 3D turbulent structures. Shih and Liu[19] provide a model (Equation (16) in the noted reference) to guide the choice of the grid size or the PRNS model constant, R_{cp}. To illustrate the results presented in Figure 12, Eq. 16 in Shih and Liu[19] is reproduced here as

$$R_{cp} \geq \left(\frac{\Delta}{l_{RANS}} \right)^{4/3} \left(\frac{u^2}{u_{RANS}^2} \right)^{-2}, \tag{13}$$

where l_{RANS} are the turbulent integral length scale, which is of the order of $k^{3/2}/\varepsilon$, and Δ is the grid size. For the first-order estimations, we assume $u_{RANS} = u_{PRNS}$ in Eq. (13), and $l_{RANS} = C \cdot k^{3/2}/\varepsilon$. Figure 12 presents the lower limits of the PRNS model constants, R_{cp}, at *X/H*=2.5 with $C = 1$ and $C = 0.09$. It can be seen from this figure that the grids used may not be suitable for the PRNS calculations with $R_{cp} = 0.38$ at locations near the wall and other regions in the free-stream.

Acknowledgments

This work was supported from an Air Force SBIR Phase II contract F33615-03-C-3315, with Dr. Datta Gaitonde as Technical Monitor.

References

[1]Spalart, P.R., Jou, W.-H., Strelets, M., and Allmaras, S.R., "Comments on the feasibility of LES for wings, and on a hybrid RANS/LES approach," In Advances in DNS/LES, C.Liu and Z. Liu Eds, Greyden Press, Columbus, Ohio, 1997.

[2]Strelets, M., "Detached Eddy Simulation of Massively Separated Flows," AIAA 2001-0879.

[3]Travin, A., Shur, M., Strelets, M., and Spalart, P.R., "Detached Eddy Simulations past a circular cylinder," *Int. J. Flow, Turbulence and Combustion*, V.63, Nos.1-4, 2000, pp.293-313.

[4]Menter, F.R., Kuntz, M., and Bender, R., "A scale-adaptive simulation model for turbulent flow predictions," AIAA 2003-0767.

[5]Shih, T.-H. and Liu, N.-S., "Partially resolved numerical simulation: from RANS towards LES for engine turbulent flows," AIAA 2004-0160.

[6]Shih, T.-H. and Liu, N.-S., "A unified strategy for numerical simulation of turbulent flows," *private communication*, 2005.

[7]Girimaji, S.S., Srinivasan, R. and Jeong, E., "PANS turbulence model for seamless transition between RANS and LES: fixed-point analysis and preliminary results," 4-th ASME-JSME Joint Fluids Engineering Conferences, July 13-16, Honolulu, Hawaii.

[8]Kim, W-W., Menon, S. and Mongia, H.C., "Large-eddy simulation of a gas turbine combustor flow," *Comb. Sci. and Tech.*, Vol.143, 1999, pp.25-62.

[9]Piomelli, U., Balaras, E., Pasinato, H., Squires, K.D., and Spalart, P.R., "The inner-outer layer interface in largy-eddy simulations with wall-layer models," International Journal of Heat and Fluid Flows," 24(2003), pp.538-550.

[10]Abid, R., "Evaluation of two-equation turbulence models for predicting transitional flows," *Int. J. Engng Sci.,* Vol.32(6), 1993, pp. 831-840.

[11]Sarkar, S., "The pressure-dilation correlation in compressible flows," *Phys. Fluids* A, Vol.4, 1992, pp.2674-2682.

[12]Cai, X., O'Brien, E.E., and Ladeinde, F., "Advection of mass fraction in forced, homogeneous, compressible turbulence", *Phys. Fluids* 10(9), P.2249-, 1998.

[13]Gaitonde, D. and Visbal, M.R., "High-Order Schemes for Navier-Stokes Equations: Algorithm and Implementation intoFDL3DI", Technical Report # AFRL-VA-WP-TR-1998-3060, Air Force Research Laboratory, Wright-Patterson AFB, OH (1998).

[14]White, F.M., *Viscous Fluid Flow*, McGraw-Hill Book Company, New York, 1974.

[15]Driver, D.M. and Seegmiller, H.L., "Features of a reattaching turbulent shear layer in divergent channel flow," *AIAA Journal*, Vol.23(2), 1985, pp.163-171.

[16]Steffen Jr., C.J., "A critical comparison of several low Reynolds number k-ε turbulence models for flow over a backward-facing step," NASA TM 106173 (AIAA-93-1927), 1993.

[17]Menter, F.R., "Zonal two-equation k-omega turbulence models for aerodynamic flows," AIAA 1993-2906.

[18]Spalart, P.R., and Allmaras, S.R., "A one-equation turbulence model for aerodynamic flows," *La Rech. A'erospatiale,* V.1, 1994, pp.5-21.

[19]Shih, T.-H., Liu, N.-S. and Chen, C-L, "A strategy for very large-eddy simulation of complex turbulent flows," AIAA 2006-0175.

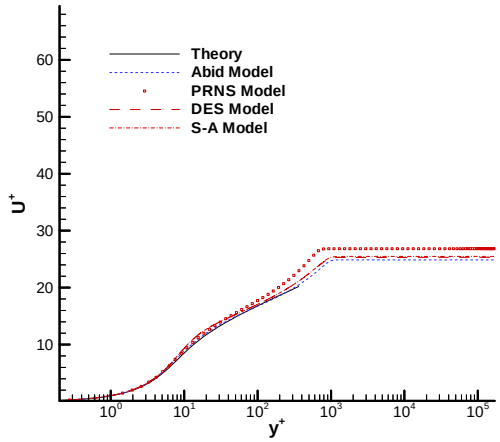

Figure 1(a): Normalized mean profile as a function of $y^+ = \rho y u^\bullet / \mu$ at $\mathrm{Re}_x = 1.5\times10^6$ for spatially-developing flat-plate boundary layer flow.

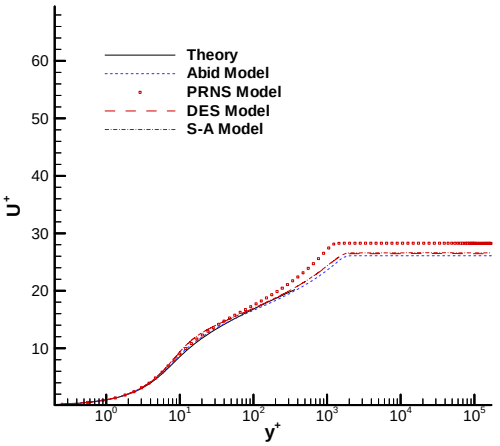

Figure 1(b): Normalized mean profile as a function of $y^+ = \rho y u^\bullet / \mu$ at $\mathrm{Re}_x = 3.0\times10^6$ for spatially-developing flat-plate boundary layer flow..

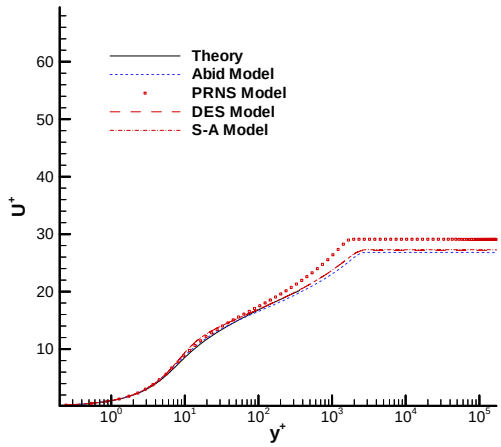

Figure 1(c): Normalized mean profile as a function of $y^+ = \rho y u^\bullet / \mu$ at $\mathrm{Re}_x = 4.5\times10^6$ for spatially-developing flat-plate boundary layer flow..

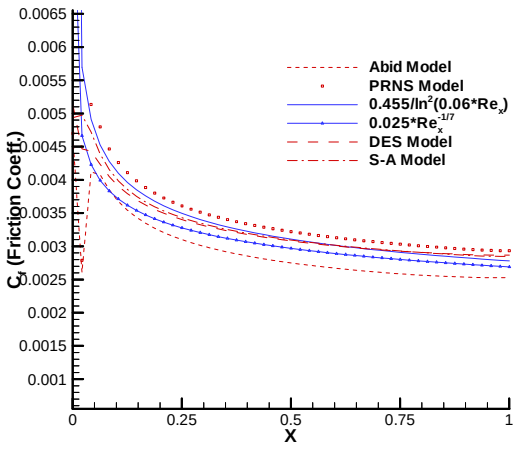

Figure 2: Comparison of numerical friction coefficients with turbulent boundary flow theory for spatially-developing flat-plate boundary layer flow.

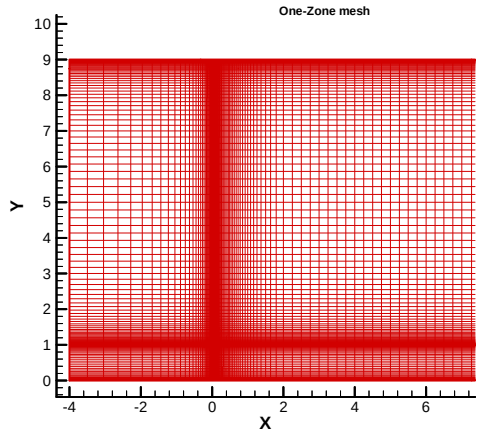

Figure 3: Mesh system for the backward-facing step flow (165×183).

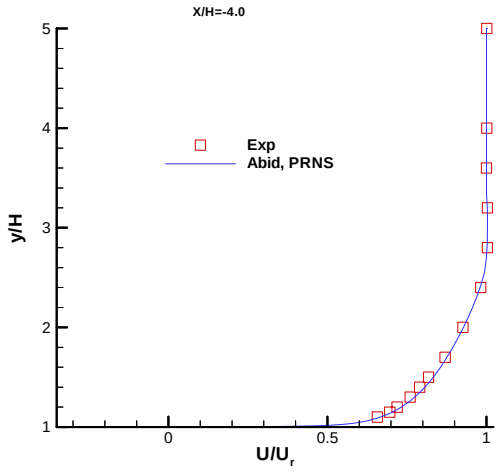

Figure 4(a): Inlet stream-wise velocity profiles for the PRNS and RANS calculations.

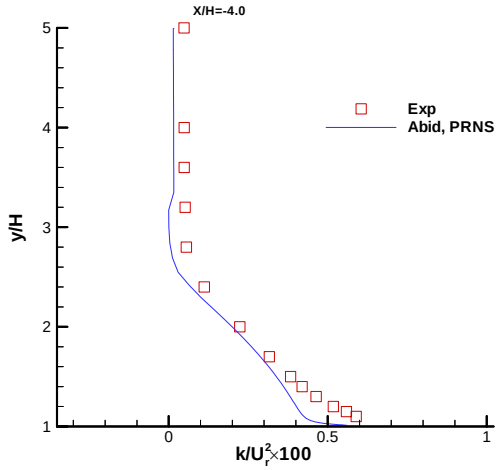

Figure 4(b): Inlet turbulent kinetic energy profile for both the PRNS and RANS calculations.

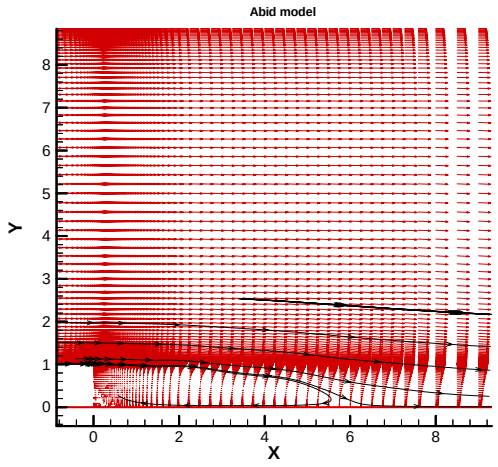

Figure 5 (a): Velocity vector plot using Abid's low-Re k-ε model.

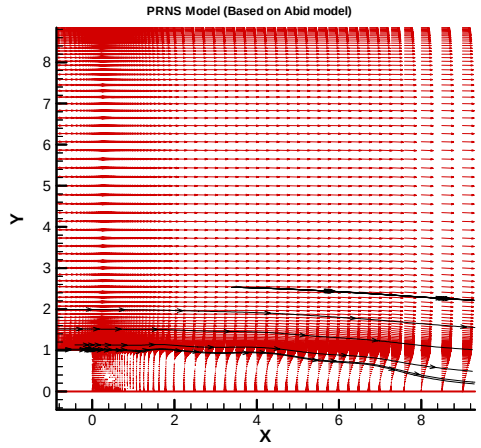

Figure 5 (b): Velocity vector plot for PRNS model based on Abid's low-Re k-ε model.

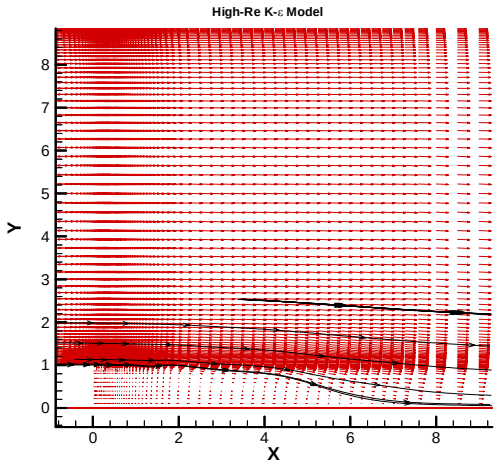

Figure 5 (c): Velocity vector plot for standard high-Re k-ε model.

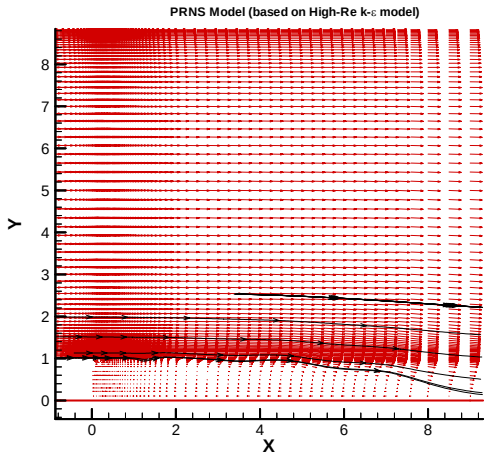

Figure 5 (d): Velocity vector plot for PRNS model based on high-Re k-ε model.

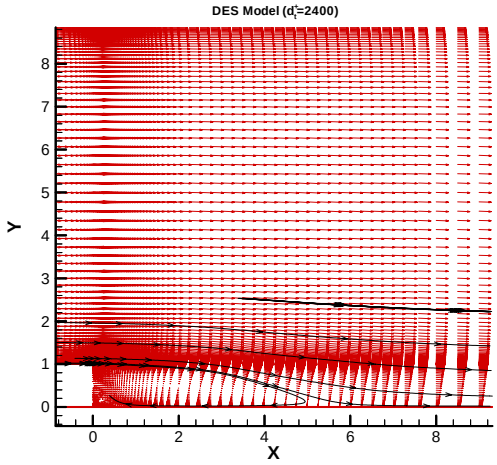

Figure 5 (e): Velocity vector plot for DES model using a big transition grid-size (d_t^+ =2400).

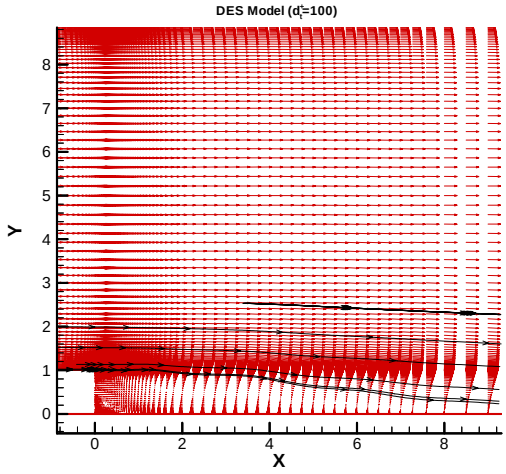

Figure 5 (f): Velocity vector plot for DES model using a small transition grid-size (d_t^+ =100).

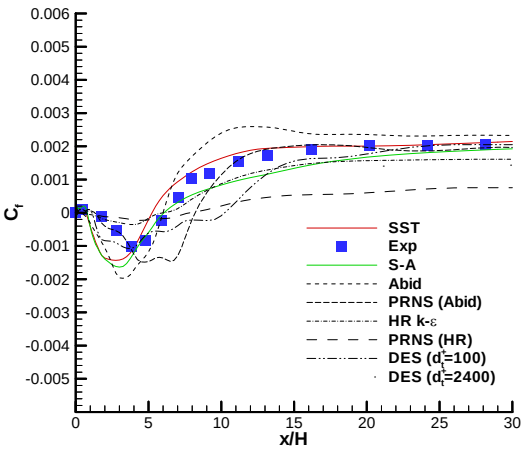

Figure 6: Friction coefficient for the step wall downstream of the step.

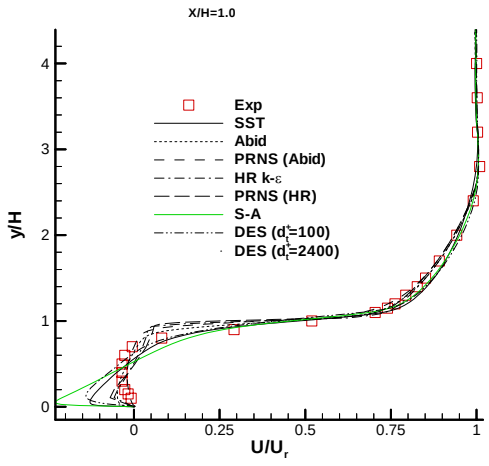

Figure 7(a): Mean velocity profiles at x/H=1.0

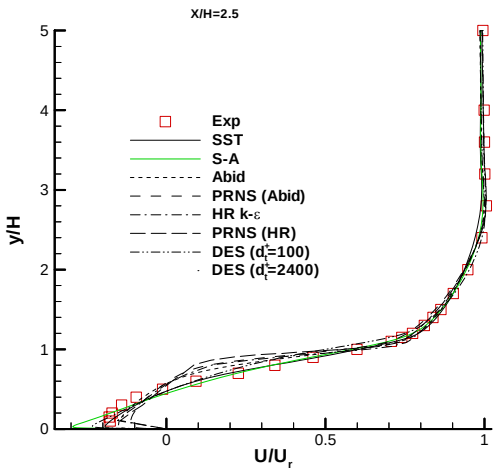

Figure 7(b): Mean velocity profiles at x/H=2.5

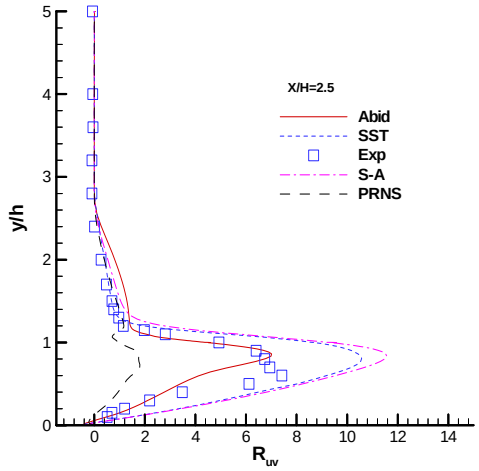

Figure 8(a): Turbulent-stress profiles at x/H=2.5 in 2D calculations

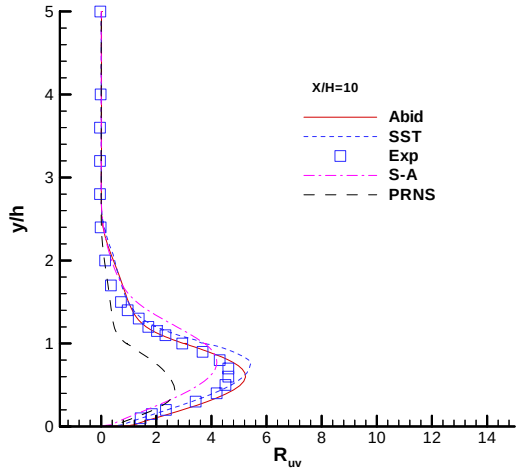

Figure 8(b): Turbulent-stress profiles at x/H=10 in 2D calculations

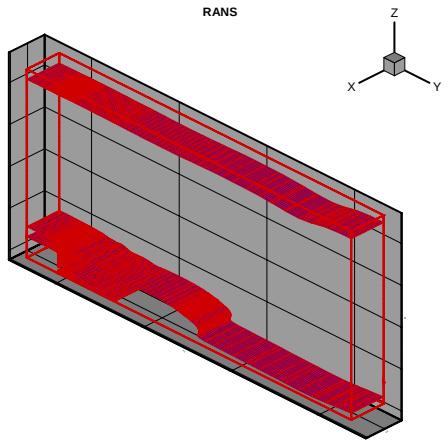

Figure 9(a): Iso-surface of vorticity ($|\omega| = 0.25$) from 3D calculations with RANS.

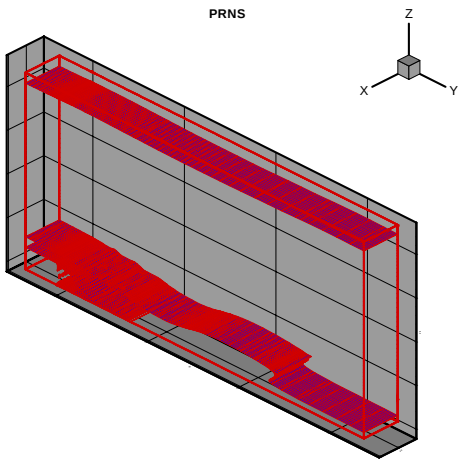

Figure 9(b): Iso-surface of vorticity ($|\omega| = 0.25$) from 3D calculations with PRNS.

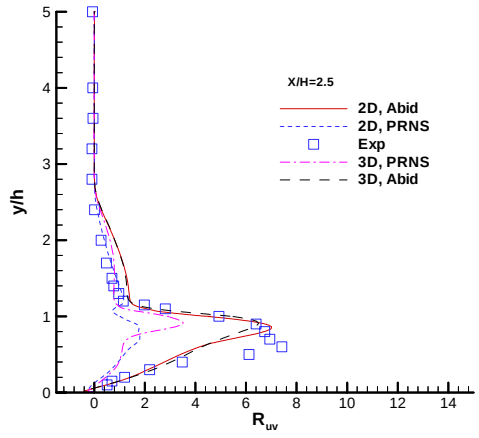

Figure 10(a): Comparison of turbulent-stress profiles at x/H=2.5.

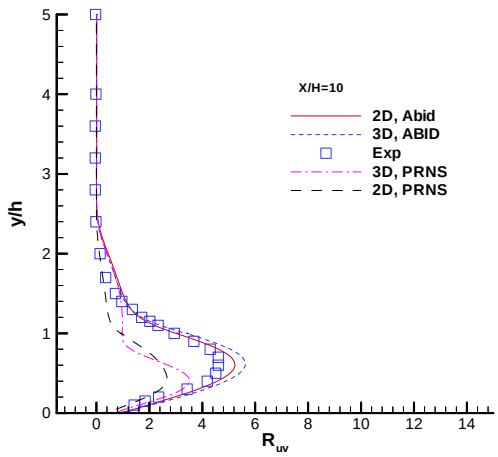

Figure 10(b): Comparison of turbulent-stress profiles at x/H=10.

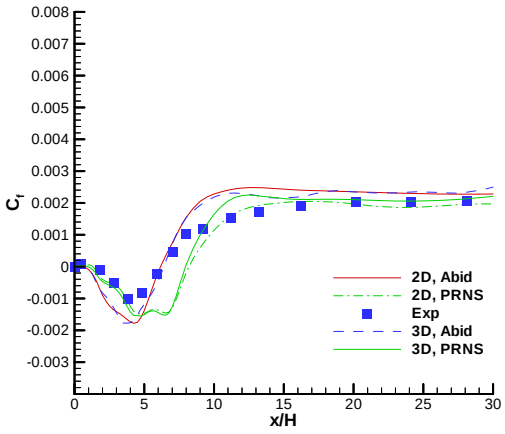

Figure 11: Comparison of the friction coefficient for the step wall downstream of the step.

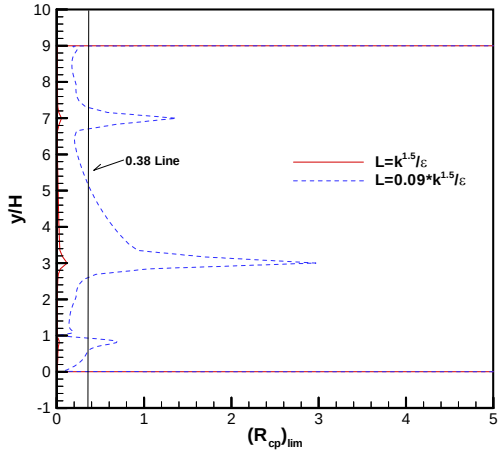

Figure 12: Distributions of the grid-size limited PRNS constants, R_{cp} at x/H=2.5.